Hindawi Publishing Corporation
Advances in Optical Technologies
Volume 2008, Article ID 254317, 7 pages
doi:10.1155/2008/254317

Research Article

Nanotomography of Cell Surfaces with Evanescent Fields

Michael Wagner,[1] Petra Weber,[1] Wolfgang S. L. Strauss,[2] Henri-Pierre Lassalle,[1,3] and Herbert Schneckenburger[1,2]

[1] *Institute of Applied Research, Hochschule Aalen, Anton-Huber-Street 1, 73430 Aalen, Germany*
[2] *Institute of Laser Technologies in Medicine and Metrology, Ulm University, Helmholtzstr. 12, 89081 Ulm, Germany*
[3] *Centre de Recherche en Automatique de Nancy, Nancy Université, CNRS, Centre Alexis Vautrin, Avenue de Bourgogne, 54511 Vandoeuvre les Nancy, France*

Correspondence should be addressed to Herbert Schneckenburger, herbert.schneckenburger@htw-aalen.de

Received 13 March 2008; Accepted 29 April 2008

Recommended by Stoyan Tanev

The technique of variable-angle total internal reflection fluorescence microscopy (TIRFM) and its application to nanotomography of cell surfaces are described. Present applications include (1) 3D imaging of chromosomes in their metaphase to demonstrate axial resolution in the nanometre range, (2) measurements of cell-substrate topology, which upon cholesterol depletion shows some loosening of cell-substrate contacts, and (3) measurements of cell topology upon photodynamic therapy (PDT), which demonstrate cell swelling and maintenance of focal contacts. The potential of the method for in vitro diagnostics, but also some requirements and limitations are discussed.

1. INTRODUCTION

Microscopy with subwavelength resolution has been a challenge for many years. While lateral resolution has been increased continuously to about 60 nm [1] in far-field microscopy and to even less in optical near-field microscopy, axial resolution has remained in a range above 100 nm. However, in close vicinity to a surface (e.g., cell-substrate interface), further improvement in axial resolution may be achieved by total internal reflection (TIR) techniques. Total internal reflection fluorescence microscopy (TIRFM) has first been described in 1981 [2], and since that time has been used increasingly for measuring cell-substrate contacts [3–5], membrane or protein dynamics [6, 7], membrane proximal ion fluxes [8] as well as endocytosis or exocytosis [9–11]. TIRFM is based on total internal reflection of a light beam propagating through a medium of refractive index n_1 (e.g., glass substrate) and meeting a second medium of refractive index $n_2 < n_1$ (e.g., cell). Despite being totally reflected at all angles $\Theta \geq \Theta_c = \arcsin(n_2/n_1)$, the incident beam establishes an evanescent electromagnetic field E_{ev} that penetrates into the second medium and decays exponentially with the distance z from the interface. According to the relation

$$d = \left(\frac{\lambda}{4\pi}\right)\left(n_1{}^2\sin^2\Theta - n_2{}^2\right)^{-1/2}, \tag{1}$$

penetration depths d between about 60 nm and more than 200 nm are attained for its intensity $I_{ev} \sim {E_{ev}}^2$, depending on the wavelength λ and the angle of incidence Θ. Therefore, fluorescent dyes located within or close to the plasma membrane can be examined almost selectively in living cells. In addition, upon variation of Θ, the relation

$$I_F(\Theta) = AcT(\Theta)te^{-\Delta/d(\Theta)} \tag{2}$$

between fluorescence intensity $I_F(\Theta)$, penetration depth $d(\Theta)$, and cell-substrate distance Δ has been established for fluorescent dyes (of constant quantum yield) distributed within a thin layer of thickness t [4] with A corresponding to an experimental constant, c to the local concentration of the fluorophore, and $T(\Theta) = 4\cos^2\Theta/[1 - (n_2/n_1)^2]$ to the transmission factor of incident light through the cell-substrate interface (on the condition that light is

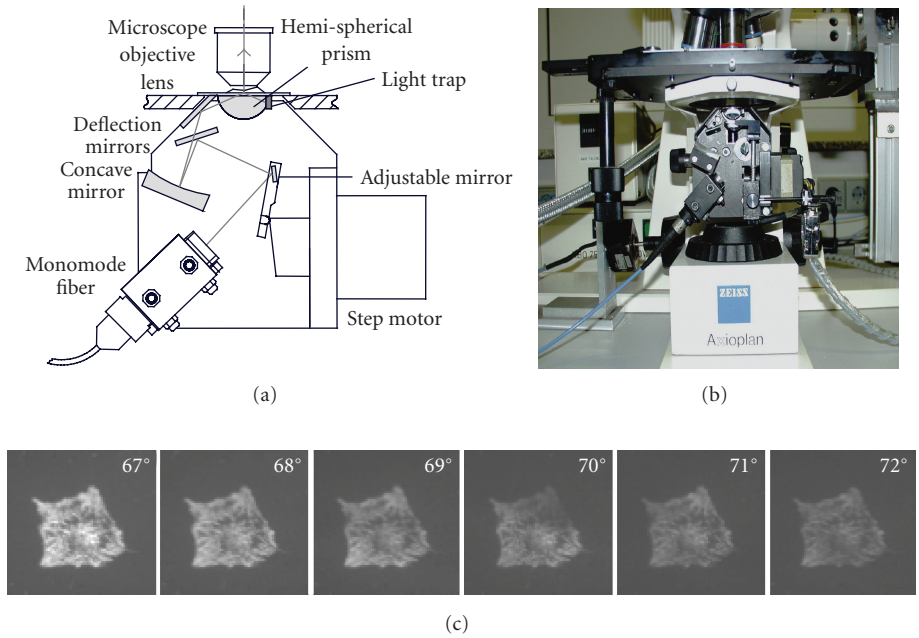

FIGURE 1: Illumination device (microscope condenser) for variable-angle TIRFM with an additional option for transillumination and phase contrast microscopy (a) scheme, (b) experimental setup, and (c) fluorescence images of the cytoplasm marker calcein in a U373MG glioblastoma cell upon variable-angle illumination.

polarized perpendicular to the plane of incidence). Similarly, a relation

$$I_F = AcT(\Theta)d(\Theta)e^{-\Delta/d(\Theta)} \tag{3}$$

has been established for fluorescent dyes distributed homogenously at distances larger than Δ [4], again assuming a constant fluorescence quantum yield over the samples.

On the basis of (2) fluorescence images of a membrane marker recorded at different angles of incidence Θ can be used to calculate the cell-substrate distance Δ with nanometre precision, when $\ln[I_F(\Theta)/T(\Theta)]$ is evaluated as a function of $d^{-1}(\Theta)$. Similarly, fluorescence images of a cytoplasm marker can be used for calculation of Δ, when $\ln[I_F(\Theta)/T(\Theta)d(\Theta)]$ is evaluated as a function of $d^{-1}(\Theta)$ according to (3). In both cases, Δ results from the slope of a straight line, which can be calculated for each pixel of a fluorescence image.

In the present paper, three examples of nanotomography with variable-angle TIRFM are given.

(1) Chromosomes in metaphase stained with the fluorescence marker DAPI are used to show the potential of 3D tomography.

(2) Human glioblastoma cells incubated with the membrane marker laurdan are used to visualize changes of cell-substrate topology upon depletion of cholesterol.

(3) Human glioblastoma cells loaded with 5-minolevulinic acid induced protoporphyrin IX are shown to change their membrane topology upon photodynamic therapy (PDT) [12].

2. MATERIALS AND METHODS

All TIRFM measurements were carried out with either chromosomes or cultivated cells. Chromosomes from Chinese hamster ovary (CHO) cells stained with the DNA marker DAPI were stopped in the metaphase of mitosis by colchicine and prepared on microscope object slides. Their typical length was about 5 μm and their diameter around 500 nm.

U373MG human glioblastoma cells obtained from the European Collection of Cell Cultures (ECACC no. 89081403) were routinely grown in RPMI 1640 medium supplemented with 10% fetal calf serum and antibiotics at 37°C and 5% CO_2. After seeding of 150 cells/mm^2, cells were grown on microscope object slides for 48 hours prior to rinsing with Earl's balanced salt solution (EBSS) and incubation for 1 hour with either the fluorescent membrane marker laurdan (8 μM) or coincubation with laurdan (8 μM) and methyl-β-cyclodextrin (MβCD; 1 mM or 4 mM) diluted in culture medium without serum. Cholesterol depletion after application of MβCD is well documented in the literature [13], and preliminary experiments proved that its intracellular amount is reduced by about 30% (at 1 mM MβCD) or 50% (at 4 mM MβCD). After incubation for 60 minutes, cells were again rinsed with EBSS and examined in the fluorescence microscope at room temperature.

In a further experiment U373MG cells cultivated under the same conditions were incubated for 6 hours at pH = 7.2 with 10^{-3} M 5-aminolevulinic acid (5-ALA; Medac Wedel, Germany), an intermediate in porphyrin biosynthesis, and rinsed with EBSS prior to TIRFM measurements. Part of the cells was transiently transfected with the plasmid encoding for the yellow fluorescent protein (YFP)-focal

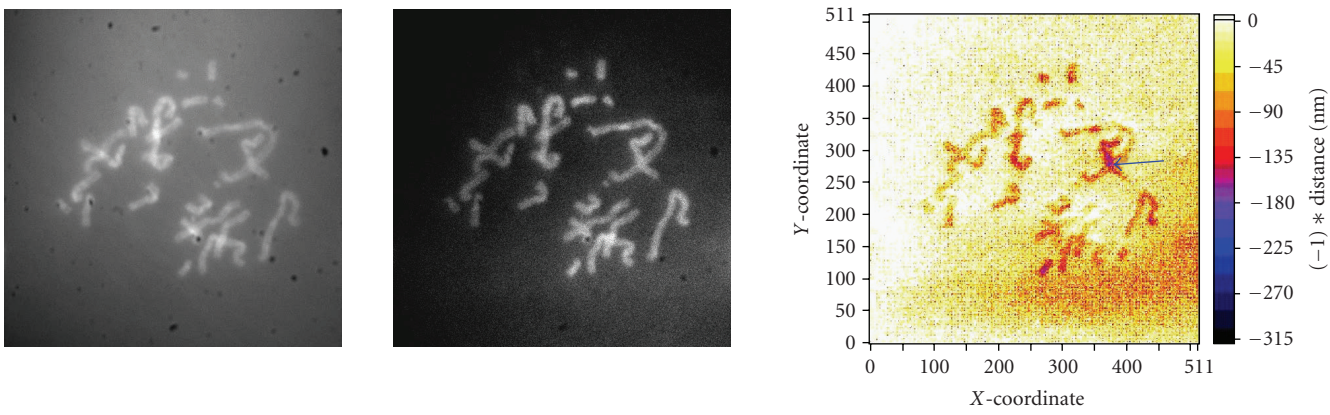

FIGURE 2: Fluorescence images of chromosomes from T47D breast cancer cells stained with DAPI in metaphase. (a) Conventional fluorescence microscopy, (b) TIRFM at $\Theta = 72.5^\circ$, and (c) tomographic imaging of chromosome-substrate distances (fluorescence excited at 391 nm and detected at $\lambda \geq 415$ nm; image size: 55 μm $\times$ 55 μm). The arrow marks overlapping chromosomes.

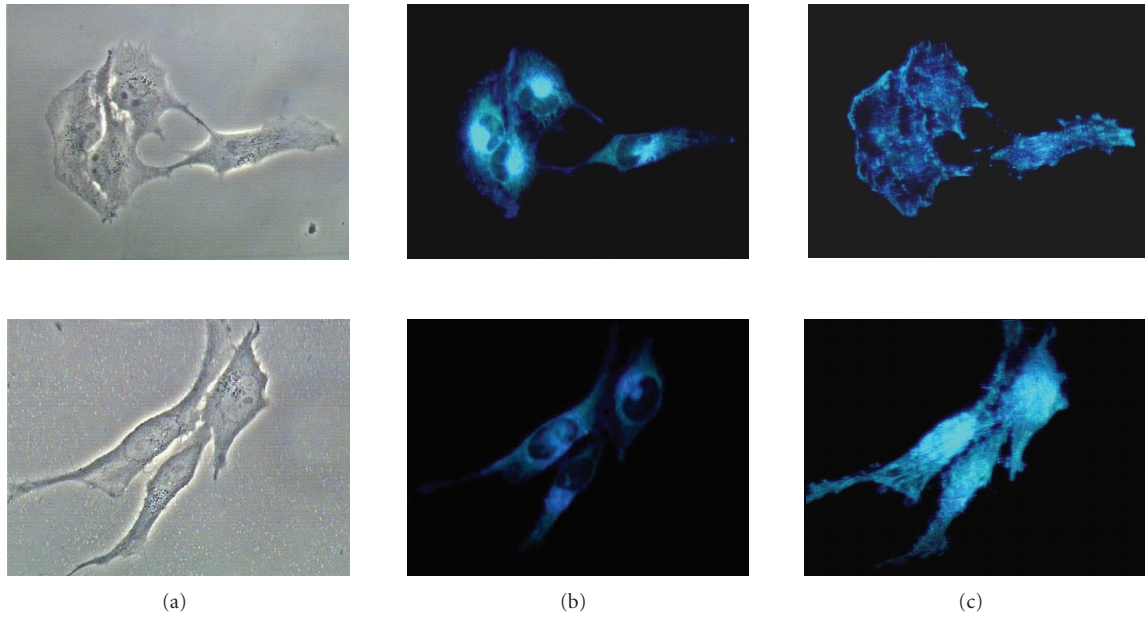

FIGURE 3: (a) Phase contrast, (b) whole cell fluorescence, and (c) TIRFM images of U373MG glioblastoma cells upon incubation with laurdan either without further treatment (upper series) or with 30% cholesterol depletion (by 1 mM MβCD; lower series). Fluorescence excited at 391 nm and detected at $\lambda \geq 415$ nm; image size: 200 μm $\times$ 150 μm. Real colour images recorded with a 3-chip CCD camera.

adhesion kinase (FAK) fusion protein [14] by lipofection (FuGene 6 Transfection Reagent, Roche Diagnostics GmbH, Mannheim, Germany) in order to visualize focal adhesions. The YFP-FAK vector was kindly provided by A.R. Horwitz, University of Virginia, USA.

For TIR illumination of cultivated cells a UV-laser diode (LDH 400 with driver PDL 800-B, Picoquant, Berlin, Germany; wavelength: 391 nm, pulse energy: 12 pJ, repetition rate 40 MHz, average power: 0.5 mW) was adapted to a fluorescence microscope (Axioplan 1, Carl Zeiss Jena, Germany) by single mode fibre optics (Point Source, kineFlex-p-3-S-395, Southampton, UK). For measurements of DAPI stained chromosomes, the 391 nm laser diode was replaced by a diode of the same type, but emitting light at 375 nm. EYFP-FAK was illuminated by the 514 nm line of an argon ion laser operated at 10 mW (Innova 90, Coherent, Santa Clara, USA). TIR illumination was carried out with a custom made device [4] permitting to vary the angle of incidence in steps of 0.5° with a resolution of 0.15°. Angles were varied either between 66° and 72° (U373MG cells) or between 70° and 76° (chromosomes). Assuming refractive indices $n_1 = 1.515$ (glass substrate) and $n_2 = 1.37$ (cytoplasm), penetration depths of the evanescent electromagnetic field within cells varied between about 160 nm and 70 nm according to (1). Fluorescence images were recorded with an electron multiplying (EM-) CCD camera with Peltier cooling and

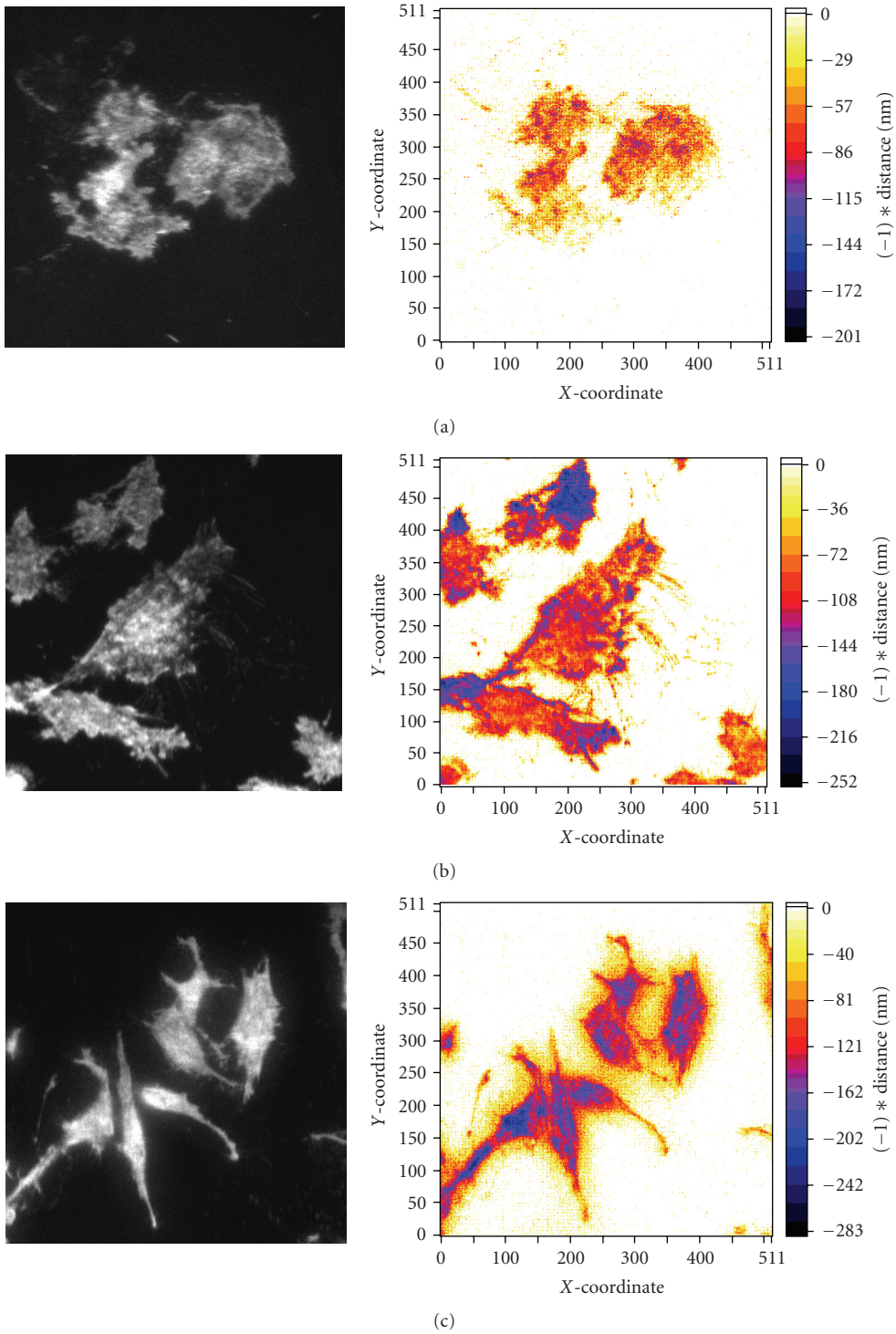

FIGURE 4: TIRFM images recorded at $\Theta = 66^{\circ}$ (left) and cell-substrate topology (right) of U373MG glioblastoma cells upon incubation with laurdan either (a) without further treatment or 30% cholesterol depletion (by 1 mM MβCD; (b) or (c) 50% cholesterol depletion (by 4 mM MβCD). Fluorescence excited at 391 nm and detected at $\lambda \geq 415$ nm; image size: 210 μm $\times$ 210 μm).

a sensitivity below 10^{-17} W/Pixel (DV887DC-BV, ANDOR Technology, Belfast, UK). In one case, this camera was replaced by a Sony 3CCD Colour Camera (Model MC-3254, AVT Horn, Aalen, Germany, in combination with the software AxioVision, Carl Zeiss Jena, Germany). A long pass filter for $\lambda \geq 415$ nm was used for detection of DAPI stained chromosomes as well as for laurdan, whereas a long-pass filter for $\lambda \geq 590$ nm was used for detection of 5-ALA induced protoporphyrin IX (PP IX), and a bandpass filter for 529 ± 20 nm (in combination with a notch filter at 514 nm)

was used for YFP-FAK. For experiments on photodynamic therapy sublethal light doses of 4 J/cm^2 at 633 nm (resulting from a 25 mW helium-neon laser; Stabilite 124B, Spectra Physics, Mountain View, USA) were applied under epi-illumination, and recording of TIRFM images was repeated immediately afterwards.

Cell-substrate distances were calculated according to (2) or (3) with a custom made computer program from a series of 8−12 TIRFM images each. For each image, the background of the camera system was subtracted. Cell-substrate distances (or chromosome-substrate distances) were evaluated for all pixels, where fluorescence intensity exceeded this background level. The scheme and the experimental setup of the TIR illumination device are depicted in Figure 1 together with a series of variable-angle TIRFM images of U373MG cells loaded with the cytoplasm marker calcein.

3. RESULTS AND DISCUSSION

3.1. 3D topology of chromosomes

Fluorescence images of DAPI stained chromosomes on a microscope slide are depicted in Figure 2 upon epi-illumination (conventional fluorescence microscopy) and TIR illumination at $\Theta = 72.5°$. Upon TIR illumination, a pronounced increase of the signal-to-background ratio occurs. Figure 2 also shows a topographic image calculated according to (3) from variable-angle TIRFM images (since the fluorescent dye is distributed over the whole chromosomes, the same fitting algorithm as for a cytoplasm marker is used). According to this topographic image, the distance between the chromosomes and the glass surface varies between 0 nm and 150 nm. Only when chromosomes are overlapping (marked by an arrow) larger distances are observed. In Figure 2, the axial resolution is far below 100 nm and typically reaches values around 10–20 nm.

3.2. Impact of cholesterol on cell-substrate topology

The fluorescence marker 6-dodecanoyl-2-dimethylamino-naphthalene (laurdan) is described in the literature as a polarity-sensitive probe, whose optical spectra depend on membrane stiffness and fluidity [15, 16]. Its fluorescence spectrum is composed by two emission bands with maxima around 440 nm and 490 nm, respectively. It is well documented that with decreasing membrane stiffness the long-wave 490 nm band becomes more pronounced compared to the short-wave 440 nm band, for example, upon temperature increase or cholesterol depletion [17]. The effect of cholesterol depletion on laurdan fluorescence in whole cells and plasma membranes is documented in Figure 3 upon (b) epi-illumination and (c) TIR illumination by real colour imaging. For a comparison, (a) phase contrast images of these cells are added. Upon incubation of the cells with laurdan (without any further treatment) the fluorescence images appear dark blue, since they are dominated by the 440 nm band, whereas upon coincubation with laurdan and MβCD (30% cholesterol depletion) whole cells still appear dark blue, whereas the plasma membranes appear blue-green due to an increasing contribution of the 490 nm band at decreasing membrane stiffness.

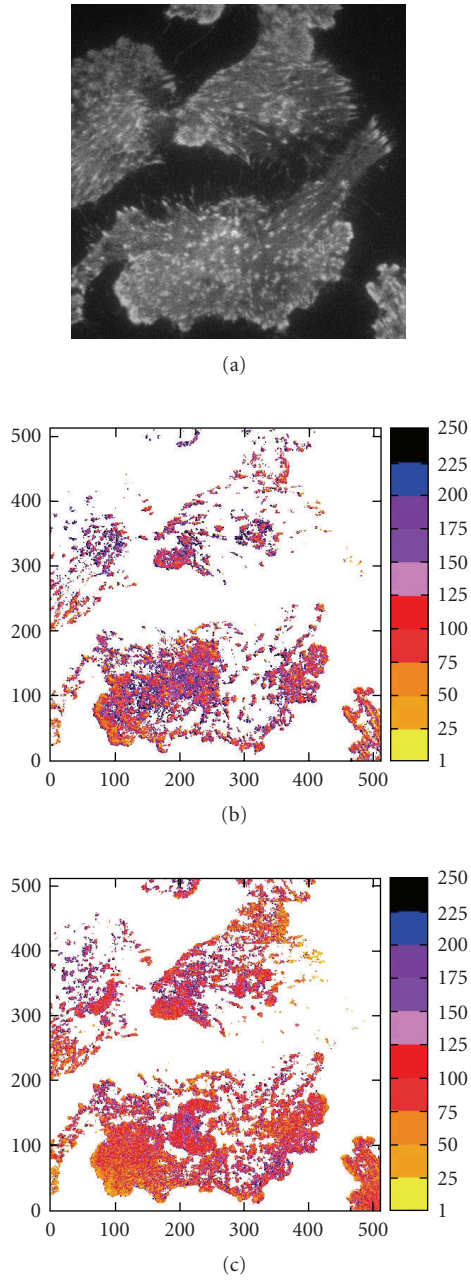

Figure 5: TIRF image of 5-ALA induced PP IX (A, $\Theta = 66°$) as well as (b) cell-substrate topology prior and (c) after PDT (633 nm; 4 J/cm^2). Fluorescence excited at 391 nm and detected at $\lambda \geq 590$ nm; image size: 140 μm × 140 μm; cell-substrate distances (colour scale) given in nanometres. Reproduced from [5] with modifications.

The question now arises how cell-substrate topology is affected by cholesterol depletion. This effect is well illustrated in Figure 4. First, upon incubation with laurdan but without any further treatment, cell-substrate distances vary between about 20 nm and 120 nm. Upon application of 1 mM MβCD

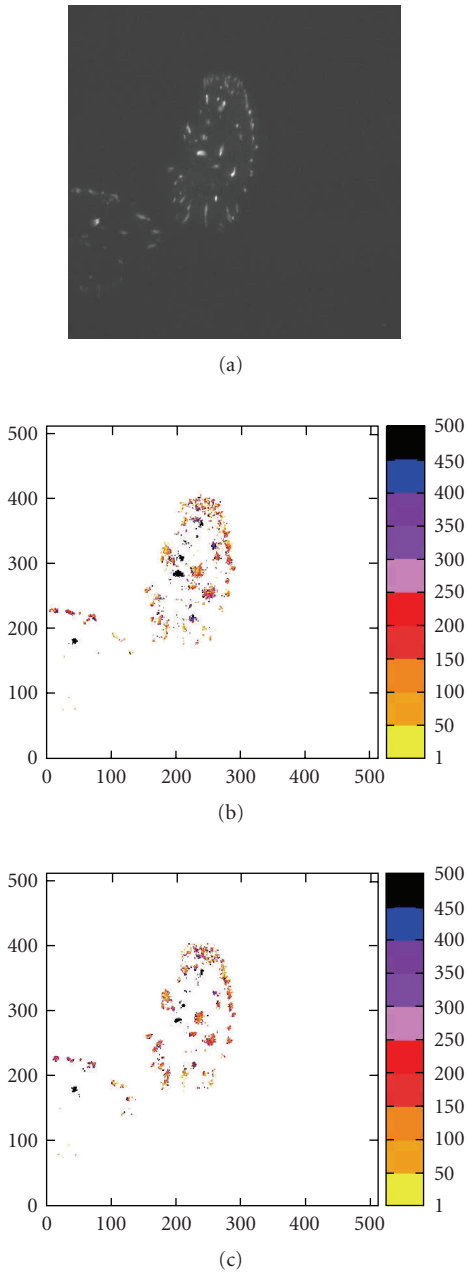

FIGURE 6: TIRF image of YFP-FAK (A, $\Theta = 66^\circ$) as well as (b) topology of focal adhesions prior and (c) after PDT with ALA-induced PP IX (633 nm; 4 J/cm^2). Fluorescence excited at 514 nm and detected at 520−550 nm; image size: 140 μm × 140 μm; cell-substrate distances (colour scale) given in nanometres.

(30% cholesterol depletion) cell-substrate distances generally increase, and upon application of 4 mM MβCD (50% cholesterol depletion), these distances are above 200 nm in the central parts of the cells, whereas on the cell edges the smaller distances are maintained. This proves that cell-substrate contacts are loosened in the central parts of the cells, which finally may lead to dissolution of the cells.

3.3. *Cell-substrate topology upon photodynamic therapy*

Adhesion of tumour cells upon photodynamic therapy (PDT) [18, 19] is an important question with regard to a possible formation of metastases. Therefore, variable-angle TIRFM appears very promising for investigation of cell-substrate topology and focal adhesions. Since 5-ALA induced protoporphyrin IX (PP IX) is partly located in the plasma membrane, it can be used as a photosensitizer as well as a membrane marker permitting to calculate cell-substrate distances according to (2). While Figure 5(a) shows a TIRFM image ($\Theta = 66^\circ$) of U373MG glioblastoma cells incubated with 5-ALA, Figure 5(b) shows cell-membrane topology before, and Figure 5(c) after application of a nonlethal light dose of 4 J/cm^2 (633 nm). While cell-substrate distances between 100 nm and 150 nm are the most frequent ones before PDT, these distances are decreasing after PDT, probably due to an increase of the cell volume upon swelling. If, instead of the plasma membrane, focal adhesions are visualized by YFP-FAK, it becomes evident from Figure 6 that these focal adhesions are maintained upon PDT. While Figure 6(a) shows a TIRFM image of focal adhesions, Figures 6(b) and 6(c) show their topologies prior and after PDT, which obviously are almost equal. Results described for PP IX and YFP-FAK have recently been verified with a larger number of U373MG glioblastoma cells and HeLa cervix cancer cells [5], proving that detachment of these cells from their substrate upon photodynamic therapy is unlikely to occur.

4. CONCLUSION

The potential of cell-substrate tomography with nanometre resolution has been demonstrated for 3 examples. Variable-angle TIRFM seems to be an ideal method, if a fluorescent dye is distributed rather homogenously either within a thin layer (e.g., cell membrane) or on top of a layer (e.g., within the cytoplasm or an isolated chromosome). A user-friendly two-layer model was applied for all calculations reported above, although up to 4 layers (glass substrate, buffer solution, cell membrane, cytoplasm) may interfere. However, for thin cell membranes, and cell-substrate distances which are smaller than the laser wavelength, the two-layer model still holds with only few percent of error [20]. Similarly, the error resulting from an inhomogeneous spot of incident light may become negligible, if this spot is large compared to the object field [4]. Further requirements for calculation of tomographic images are a stationary spot of illumination (upon variation of the angle Θ), a constant fluorescence quantum yield over the measured parts of the sample (as deduced in the case of laurdan from the homogeneous distribution of fluorescence lifetimes) and a high signal-to-noise ratio. Since TIRFM images are usually about 100 times weaker than conventional fluorescence images, a high sensitivity of the detection system, for example, of an EM-CCD camera, is needed. This kind of detection system also permits the use of very low illumination doses (far below 1 J/cm^2 for 10−12 TIRFM images), which may assure

cell survival in high-resolution microscopy and in vitro diagnostics.

ACKNOWLEDGMENTS

This project was funded by the Bundesministerium für Bildung und Forschung (BMBF; Grant no. 1701B04). Technical assistance by Claudia Hintze is gratefully acknowledged.

REFERENCES

[1] K. I. Willig, B. Harke, R. Medda, and S. W. Hell, "STED microscopy with continuous wave beams," *Nature Methods*, vol. 4, no. 11, pp. 915–918, 2007.

[2] D. Axelrod, "Cell-substrate contacts illuminated by total internal reflection fluorescence," *The Journal of Cell Biology*, vol. 89, no. 1, pp. 141–145, 1981.

[3] G. A. Truskey, J. S. Burmeister, E. Grapa, and M. W. Reichert, "Total internal reflection fluorescence microscopy (TIRFM). II. Topographical mapping of relative cell/substratum separation distances," *Journal of Cell Science*, vol. 103, no. 2, pp. 491–499, 1992.

[4] K. Stock, R. Sailer, W. S. L. Strauss, M. Lyttek, R. Steiner, and H. Schneckenburger, "Variable-angle total internal reflection fluorescence microscopy (VA-TIRFM): realization and application of a compact illumination device," *Journal of Microscopy*, vol. 211, no. 1, pp. 19–29, 2003.

[5] H.-P. Lassalle, H. Baumann, W. S. L. Strauss, and H. Schneckenburger, "Cell-substrate topology upon ALA-PDT using variable-angle total internal reflection fluorescence microscopy (VA-TIRFM)," *Journal of Environmental Pathology, Toxicology and Oncology*, vol. 26, no. 2, pp. 83–88, 2007.

[6] N. L. Thompson, A. W. Drake, L. Chen, and W. Vanden Broek, "Equilibrium, kinetics, diffusion and self-association of proteins at membrane surfaces: measurement by total internal reflection fluorescence microscopy," *Photochemistry and Photobiology*, vol. 65, no. 1, pp. 39–46, 1997.

[7] S. E. Sund and D. Axelrod, "Actin dynamics at the living cell submembrane imaged by total internal reflection fluorescence photobleaching," *Biophysical Journal*, vol. 79, no. 3, pp. 1655–1669, 2000.

[8] A. Demuro and I. Parker, "Imaging the activity and localization of single voltage-gated Ca^{2+} channels by total internal reflection fluorescence microscopy," *Biophysical Journal*, vol. 86, no. 5, pp. 3250–3259, 2004.

[9] W. J. Betz, F. Mao, and C. B. Smith, "Imaging exocytosis and endocytosis," *Current Opinion in Neurobiology*, vol. 6, no. 3, pp. 365–371, 1996.

[10] M. Oheim, D. Loerke, W. Stühmer, and R. H. Chow, "The last few milliseconds in the life of a secretory granule. Docking, dynamics and fusion visualized by total internal reflection fluorescence microscopy (TIRFM)," *European Biophysics Journal*, vol. 27, no. 2, pp. 83–98, 1998.

[11] S. S. Licht, A. Sonnleitner, S. Weiss, and P. G. Schultz, "A rugged energy landscape mechanism for trapping of transmembrane receptors during endocytosis," *Biochemistry*, vol. 42, no. 10, pp. 2916–2925, 2003.

[12] T. J. Dougherty, "Photosensitizers: therapy and detection of malignant tumors," *Photochemistry and Photobiology*, vol. 45, no. 6, pp. 879–889, 1987.

[13] A. E. Christian, M. P. Haynes, M. C. Phillips, and G. H. Rothblat, "Use of cyclodextrins for manipulating cellular cholesterol content," *Journal of Lipid Research*, vol. 38, no. 11, pp. 2264–2272, 1997.

[14] D. J. Webb, K. Donais, L. A. Whitmore, et al., "FAK-Src signalling through paxillin, ERK and MLCK regulates adhesion disassembly," *Nature Cell Biology*, vol. 6, no. 2, pp. 154–161, 2004.

[15] T. Parasassi, E. K. Krasnowska, L. A. Bagatolli, and E. Gratton, "Laurdan and prodan as polarity-sensitive fluorescent membrane probes," *Journal of Fluorescence*, vol. 8, no. 4, pp. 365–373, 1998.

[16] L. A. Bagatolli, T. Parasassi, G. D. Fidelio, and E. Gratton, "A model for the interaction of 6-lauroyl-2-(*N*,*N*-dimethylamino)naphthalene with lipid environments: implications for spectral properties," *Photochemistry and Photobiology*, vol. 70, no. 4, pp. 557–564, 1999.

[17] P. Weber, M. Wagner, and H. Schneckenburger, "Microfluorometry of cell membrane dynamics," *Cytometry Part A*, vol. 69, no. 3, pp. 185–188, 2006.

[18] N. Rousset, V. Vonarx, S. Eléouet, et al., "Effects of photodynamic terapy on adhesion molecules and metastasis," *Journal of Photochemistry and Photobiology B*, vol. 52, no. 1–3, pp. 65–73, 1999.

[19] A. Uzdensky, E. Kolpakova, A. Juzeniene, P. Juzenas, and J. Moan, "The effect of sub-lethal ALA-PDT on the cytoskeleton and adhesion of cultured human cancer cells," *Biochimica et Biophysica Acta*, vol. 1722, no. 1, pp. 43–50, 2005.

[20] W. M. Reichert and G. A. Truskey, "Total internal reflection fluorescence (TIRF) microscopy. I. Modelling cell contact region fluorescence," *Journal of Cell Science*, vol. 96, no. 2, pp. 219–230, 1990.